Supporting information for the paper:

Homology model and docking-based virtual screening for ligands of the σ_1 receptor

*Erik Laurini, Valentina Dal Col, Maria Grazia Mamolo, Daniele Zampieri, Paola Posocco, Maurizio Fermeglia, Luciano Vio, Sabrina Pricl**

[a]Molecular Simulation Engineering (MOSE) Laboratory, Department of Industrial Engineering and Information Technology (DI3), University of Trieste, Via Valerio 10, 34127 Trieste, Italy
[b]Department of Chemical and Pharmaceutical Sciences, University of Trieste, 34127 Trieste, Italy

Content

S1. General methodology

The general methodology for structural modeling of the σ_1 receptor adopted in the present work is summarized in Figure S1. Accordingly, the initial homology model of the target protein is optimized by including information about bioactive ligands as spatial restraints. The validity of the final model is then checked by scoring the protein/ligand complexes via MM/PBSA calculations. Lastly, the protein model is employed as a platform for structure-based drug design.

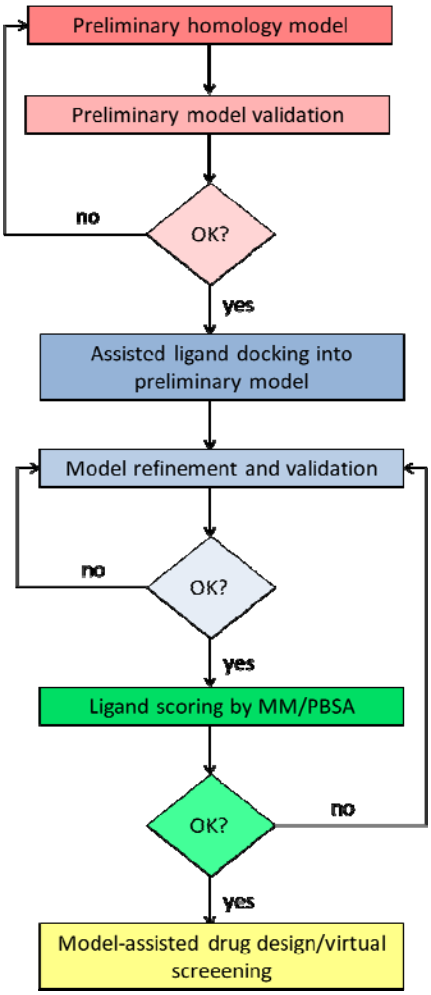

Figure S1. Flowchart of the ligand information-based homology modeling methodology applied in this work to σ_1 receptor.

S2. Prediction of the σ_1 receptor transmembrane (TM) regions and secondary structure

For the identification of the transmembrane (TM) helical domains and the prediction of the overall secondary structure of the σ_1 receptor, we employed the programs TMPRED,[1] DISOPRED,[2] Predict Protein,[3] HMMTOP,[4] I-TASSER,[5] and the *Secondary Structure Prediction* tool of *Discovery Studio* (*DS*) (v. 2.1, Accelrys, San Diego, USA) in a comparative fashion.

All programs identified the same three TM domains, spanning the protein residues 10-30, 80-100, and 180-200, respectively. A prediction of the secondary structure of the entire protein was also obtained by running different programs and comparing the corresponding output for quality, reliability, and matching. Again, very similar results were obtained, according to which the σ_1 secondary structure should feature, aside the already described TM domains, a few β-strands in the C-terminal half (residues 111-116, 133-135, 144-146, and 158-164), and some loops, as shown in Figure S2.

Figure S2. General secondary structure prediction of the σ_1 receptor. The main protein structural motifs (a-helices, b-sheets, and loop/coils) are highlighted below the primary sequence as follows: orange/red large tubes: α-helices; light blue arrows: β-sheets; gray thin tubes: loops/coils.

S3. Template searching, initial σ_1 receptor 3D model building, and preliminary model validation

The primary sequence of the σ_1 receptor was obtained from SWISS-PROT database (accession number Q99720).[6] A comparative PSI-Blast search against the non-redundant protein database via the NCBI website (http://www.ncbi.nlm.nih.gov), the ExPASy Proteomic Server (http://expasy.org), and MODWEB (http://modbase.compbio.ucsf.edu/scgi/modweb.cgi) did not identify one single protein with high homology for the target receptor sequence, as expected. However, all these searches retrieved 4 different protein sequences having both a considerable similarity (≥ 30%) with specific portions of the σ_1 sequence and an X-ray structure available. The sequence alignment between the receptor target sequence and the templates was conducted automatically by applying different scoring matrices, gap penalties, and gap length penalty parameters in order to achieve the highest sequence homology. In detail: i) cold-aminopeptidase (PDB code 3CIA)[7] gave 22% sequence identity (SI) and 37% sequence similarity (SS) between residues 432-458 and σ_1 residues 17-43; ii) Udp-Sulfoquinovose Synthase (PDB code 1I24)[8] featured 17% SI and 31% SS between residues 58-186 and σ_1 residues 44-156; iii) for Tk-subtilisin (PDB code 2Z2Z),[9] 366-396 residues shared 39% SI and 55% SS with σ_1 residues 157-187; and iv) pyruvate dehydrogenase kinase isoform 3 (PDB code 2Q8I)[10] residues 140-178 yielded 42% SI and 55% SS with residues 188-223 of the σ_1 receptor (see Figure S3).

Accordingly, the crystal structures of these 4 proteins were used as templates for building the different sections of the σ_1 homology structure. Each initial template-based structure was obtained

using MODWEB, was checked using the *Build Homology Models* of DS, and compared to the corresponding template through the *Structure Comparison -> Match Maker* feature of *Chimera.*[11]

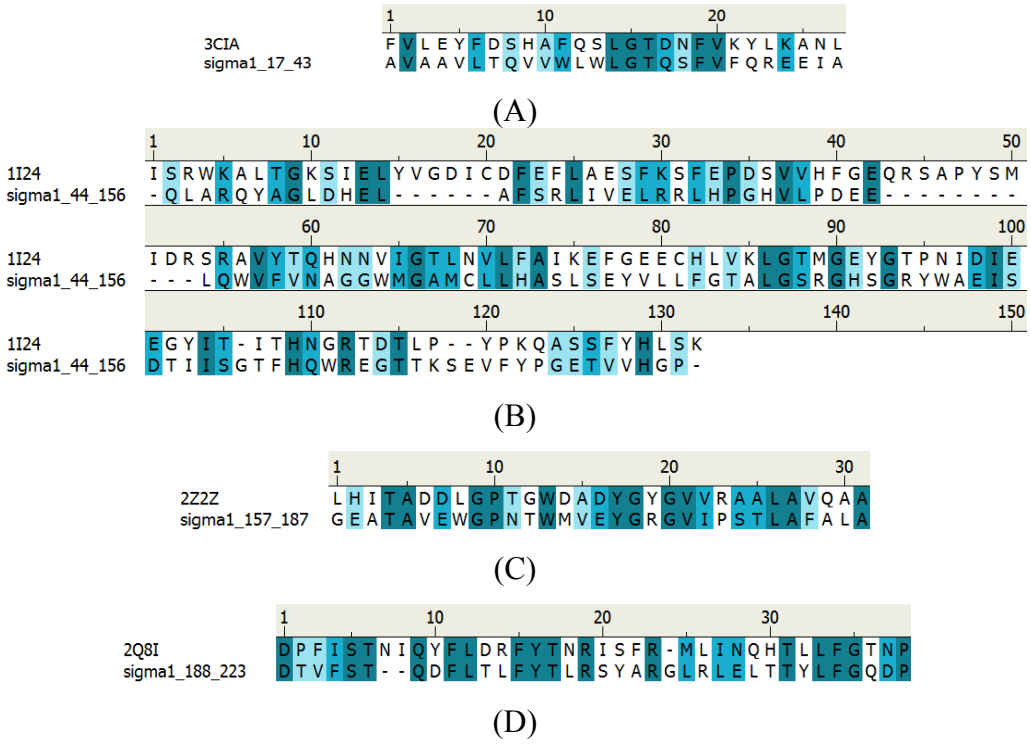

Figure S3. Sequence alignment of different portions of the human σ_1 receptor with : (A) cold-aminopeptidase (PDB code: 3CIA)[7]; (B) Udp-Sulfoquinovose Synthase (PDB code 1I24)[8]; (C) Tk-subtilisin (PDB code 2Z2Z)[9]; and (D) pyruvate dehydrogenase kinase isoform 3 (PDB code 2Q8I)[10].

The first part of the N-terminal domain of the protein (residues 1-16) showed no homology with any other protein in all queried databases; therefore, it was built *de novo* using the *Build and Edit Protein* modulus of *DS*. Finally, the overall receptor 3D structure was built linking the different template-based homology models and creating/optimizing the missing loop portions via several refinement processes. In details, the different protein fragments were jointed according to the following sequential procedure: i) for each junction zone, 400 different models were generated using the *Loop Refinement* modulus of the MODELER suite implemented in *DS*; ii) all generated models were checked and ranked for quality coupling conformational (i.e., Ramachandran plot) and energetical criteria (i.e., energy minimization using the *DS* CHARMm program); and iii) the best ranking solution according to both criteria within the entire set of generated models was finally selected. The resulting structure was further adjusted manually to fully match the results of secondary structure predictions and optimized for side chain conformation. The stereochemistry quality of the resulting model was checked using *PROCHECK,*[12] *WHATIF*,[13] and *PROSA.*[14] The analysis of the Ramachandran plot produced by *PROCHECK* of the main torsional angles of the

preliminary model revealed that a total of 95.8% of the protein residues were in the most favored regions of the plot, with 2.7% in additionally allowed regions, giving a total of 98.5%. Bond lengths and angles were all found within their normal range, and no bumps (corresponding to high van der Waals energies) were detected. Other stereochemical parameters, such as peptide planarity, bad nonbonded interactions, main-chain hydrogen bonding energy, and standard deviations of χ_1 angle (i.e., the first torsion angle of the side chains) were also examined and checked for validity. Accordingly, the total quality G-factor was – 0.27, revealing the good quality of the initial σ_1 model structure since reasonable values for the G-factor in *PROCHECK* fall between 0 and – 0.5, with the best models displaying values closest to 0. The packing quality of the 3D model was assessed for the absence of steric clashes between any pair of atoms. The results of the *WHATIF* quality report showed a normality index (z-score) of -1.89, a value which falls in the acceptable range for a valid structure (z-score > -5.0). The analysis of the *PROSA* results revealed that, for most regions in the initial σ_1 model, the residue-residue interaction energies were all attractive, indicating no bad backbone contacts for the model in this regions. Lastly, the good overall quality of the model was also reflected in the corresponding value of the PROSA normalized z-score = 0.92, being z-score > 0.70 indicative of a good structure.

S4. Model refinement via molecular dynamics (MD) simulations and final model validation

The preliminary 3D homology model of the σ_1 receptor was further refined and its stability verified via a cycle of MD simulations in a pre-equilibrated POPC/TIP3P solvated membrane system[15]. All MD simulations were carried out using the *Sander* and *Pmemd* modules of the *AMBER 9* suite of programs.[16]. The σ_1 3D homology model was inserted manually into the membrane with the two transmembrane helices parallel to the *xy* plane (being *z* the direction normal to the membrane). Those lipid molecules that were found at a distance smaller than 0.5 Å from any protein atoms were removed. The system was further solvated by a TIP3P[17] box of water extending at least 10.0 Å in each direction from the solute; then, 136 Cl^- and 142 Na^+ counterions were added to ensure the overall charge neutrality of the system and to mimic a physiological ionic strength of 0.15 M. The energy of the resulting system was relaxed via a multi-step minimization procedure using the *AMBER ff03* force field,[18] as follows. First only the lipids, water molecules and counterions were minimized for 5000 cycles of steepest-descent minimization. Next, also the side chains of the σ_1 receptor were further relaxed using a 1000- cycle energy minimization to relieve possible unexpected side-chain clashes. Lastly, the whole system was energy relaxed for further 1000-cycles of conjugate-gradient minimization. The system was then gradually heated to T = 300 K in three NVT MD intervals, allowing a 20 ps interval per each 100 K, followed by NPT MD

simulations at 300 K for other 60 ps with the backbone of the protein restrained with an harmonic potential, while all lipids, water molecules, counterions, and the protein side chains were allowed to move. Then, the whole system was further equilibrated in the NVT ensemble for 15 ns at 300 K, to attain a well relaxed receptor structure and to verify the stability of the corresponding MD trajectory. The time step used in the MD simulation was 2 fs. Periodic boundary conditions were used with Berendsen temperature coupling[19] and P =1 atm, with isotropic molecule-based scaling. The SHAKE algorithm[20] was used to fix all covalent bonds containing hydrogen atoms. Long-range nonbonded van der Waals interactions were truncated by using a dual cut off of 6 and 12 Å, respectively, where energies and forces due to interactions between 6 and 12 Å were updated every 20 time steps. The particle mesh Ewald method[21] was used to treat the long- range electrostatics. A residue-based cut off of 8 Å was used for the non-covalent interactions. During the NVT MD simulations, the coordinates of the protein were saved every 1 ps.

The σ_1 model structure remained stable for all 15 ns of the MD trajectory, as indicated by the small fluctuations of the root-mean-square (RMS) deviation of the simulated position of the backbone atoms with respect to those of the initial structure and the corresponding total potential energy of the system E shown in Figure S4.

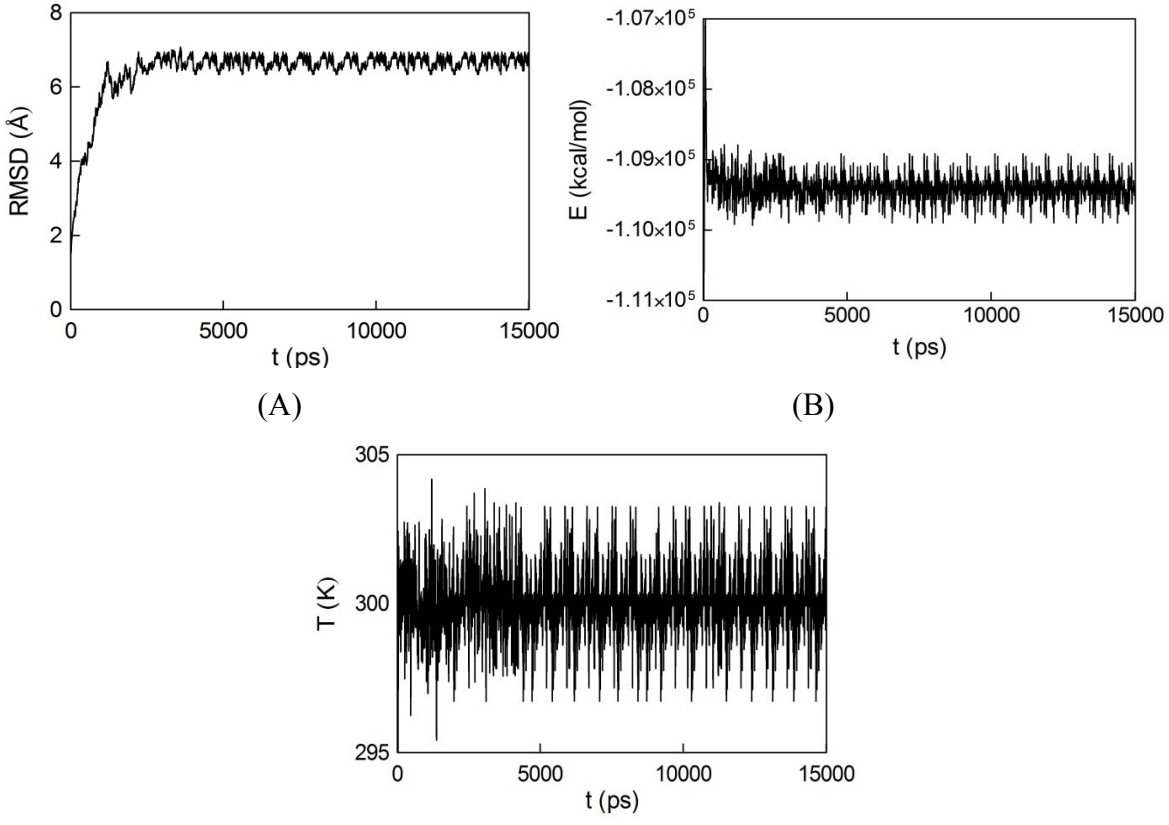

(A) (B)

(C)

Figure S4. (A) RMSD of the coordinates of the backbone atoms of the initial homology model of the σ_1 receptor along the 15 ns MD simulation compared with those of the initial structure, (B) time behavior of the total potential energy and (C) temperature of the σ_1 receptor 3D model in water during the same MD simulation.

From the above described 15 ns equilibrated MD trajectory, the protein coordinates were extracted from last frame of the membrane complex (see Figure S5), and the corresponding 3D σ_1 receptor model was evaluated for quality and reliability.

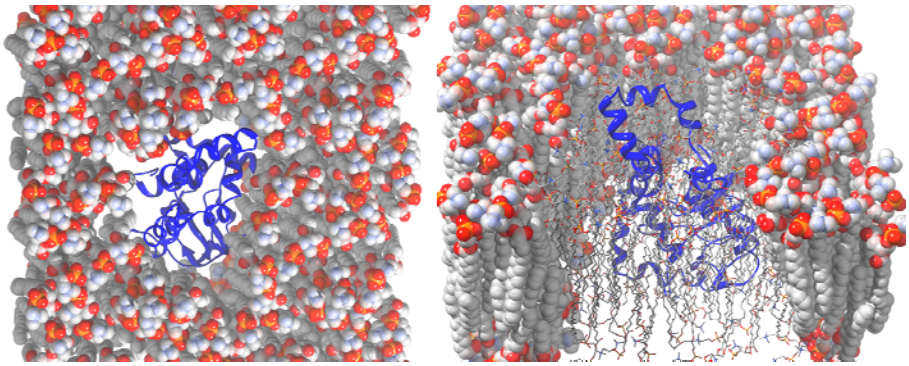

Figure S5. Top (left) and side view (right) of the last frame extracted from the equilibrated MD trajectory of the σ_1 receptor 3D homology model in a solvated membrane environment. The protein secondary structure is depicted as a blue ribbon. POPC molecules are shown as atom-colored CPK spheres. In the right panel, a mixed representation of CPK spheres and sticks was chosen to represent the lipid molecules for graphical purposes. Atom color code: O, red; C, light gray; N, light blue; H, white; P, orange. Water molecules and ions are not shown for clarity.

According to *PROCHECK*, the Ramachandran plot shows that 221 residues are found in the most favored regions, while only two residues fall in the disallowed regions (see Figure S6).

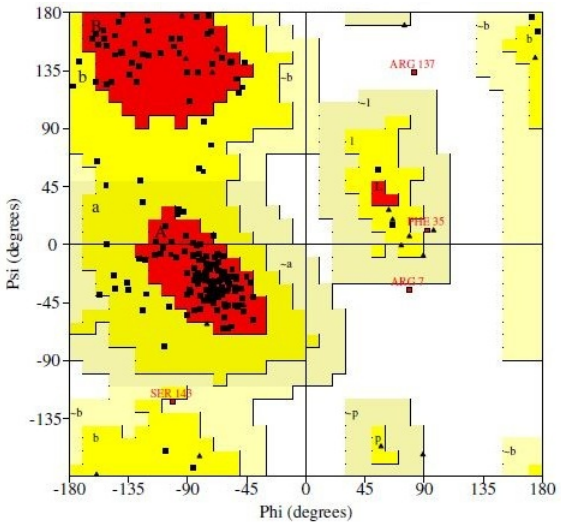

Figure S6. Ramachandran plot generated from the MD refined 3D homology model of the σ_1 receptor.

By comparison with the pre-refined structure, the G-factor increased from -0.27 to -0.21, indicating that the MD simulations relieved some bad contacts between nonbonded atoms without increasing the number of bad dihedral angles of the structure. The result of the ϕ-ψ combination displayed by the Ramachandran plot of the MD σ_1 relaxed model in Figure S5 is consistent with this change in G-factor, with a higher percentage of the residues in the most favored regions (97.9%), and a smaller number in generously allowed regions (2.1%), giving a total percentage of 100%. Other stereochemical parameters such as dihedral angles, covalent geometry, and planarity were also examined. The respective G-factor were all close to zero, and all values were well within the acceptable limits. Utterly analogous results were obtained by running *MOLPROBITY*.[22] The packing quality of the MD relaxed model was checked by the atomic contact analysis of *WHATIF*, yielding a z-score of -0.89 which testifies the improvement of the model after MD relaxation. The packing quality of each protein residue was also evaluated by the *VERIFY-3D* method:[23] the compatibility score above zero in the *VERIFY-3D* graph shown in Figure S7 is a song of side-chain environments and suggests that the model is characterized by an overall self-consistency in terms of sequence-structure compatibility. The enhancement of the overall 3D homology model quality was also reflected in the value of the corresponding *PROSA* normalized z-score of 0.98. Such high values of the *PROSA* z-score approach those typical of high resolution crystal structures, further supporting the fact that the proposed model is of very good quality in backbone conformation.

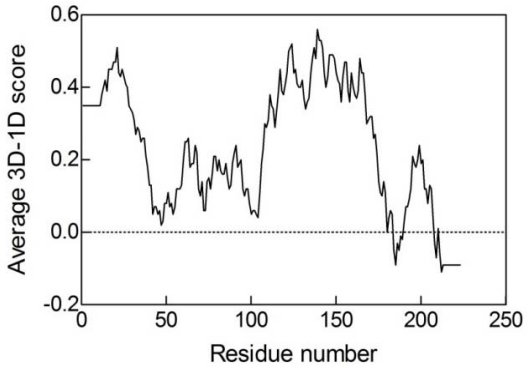

Figure S7. VERIFY-3D graph generated for the MD refined 3D homology model of the σ_1 receptor.

The overall accuracy of a comparative model is related to the percentage sequence identity on which it is based, correlating with the relationship between the structural and sequence similarity of the target and template proteins. High-accuracy comparative models are based on more than 50% sequence identity to their templates. Medium-accuracy comparative models are based on 30 to 50% SI, while low-accuracy comparative models rely on less than 30% of SI. Nonetheless, other factors such as template selection and alignment accuracy usually have a large impact on the resulting final

model quality, especially for models based on less than 40% sequence identity to the templates.[24] We are well aware of the fact that many methods often fail to correctly align protein pairs with 20-30% pairwise sequence identity, and that in the present work a consistent portion of the σ_1 receptor was modeled in this "twilight zone".[25] However, since i) it is also often possible to correctly predict features of the target protein that do not occur in the template structure, ii) errors in functional important regions in comparative models are many times relatively low because the functional regions (e.g., binding sites) tend to be more conserved in evolution than the rest of the fold, and iii) all σ_1 ligands considered were ranked for their affinity towards the σ_1 receptor 3D model developed in this work consistently with the corresponding experimental values, we are confident that the proposed homology model of this important protein is characterized by an overall correct folding.

S5. Assisted-ligand docking into the σ_1 receptor 3D homology model

To retrieve a putative binding site in the σ_1 receptor model structure we exploited the currently available preliminary information on sequence-structure relationships and mutagenesis studies,[26] and some ligand-binding pharmacophore requirements.[27] In detail, some experiments revealed that an alternative splice variant of the σ_1 receptor encoding gene lacking exon 3 expresses a protein that has no ability to bind ligands.[26] The region deleted in the splice variant consists of the protein residues 119-149. Thus, the putative membrane spanning domain should lie upstream the region coded by exon 3 and, since the transcript of this splice variant is devoid of ligand binding function, we may hypothesize that the ligand binding site may sensible reside in the C- terminal half of the protein. This region contains 12 anionic residues, among which D126 and E172 were found to be directly involved in ligand binding by mutagenesis studies.[26] Moreover, a further hydrophobicity analysis performed in the present study using *PONDR*[28] identified, aside the TM regions, a third hydrophobic region matching the SBDLII region and centered on Asp188, a residue specifically photolabeled by [125I]IACoc (3-iodo-4-azido cocaine).[29] Having localized this protein region as a possible zone for ligand binding, a thorough search for a sequence satisfying the chemical features imposed our recently developed 3D pharmacophore model[27] was performed (see Figure S8(A)), and successfully retrieved. Thus, compound **1c** was initially selected for docking into the putative σ_1 binding site. *AUTODOCK* 4[30] with *AUTODOCK TOOLS* 1.4.6 on a win64 platform was used for all docking experiments. The general docking methodology was based on a consolidated procedure;[31] accordingly, it will be described here only briefly. The size of the binding site was defined via *DISCOVERY STUDIO (DS) Studio* (v.2.1, Accelrys Inc., San Diego, CA, USA), using an opening site of 10 Å and a grid size of 0.7 Å. The *AUTODOCK* grid box dimensions, based on

the identified cavity from *DS*, were large enough to cover all possible rotations of the ligand. *AMBER* 12-6 and 12-10 Lennard-Jones parameters were used in modeling van der Waals interactions and hydrogen bonding (N-H, O-H and S-H), respectively. In the generation of the electrostatic grid maps, the distance dependent relative permittivity of Mehler and Solmajer was applied.[32] 300 hundred Monte Carlo/Simulated Annealing (MC/SA) runs were performed, with 100 constant temperature cycles for simulated annealing. For these calculations, the GB/SA implicit water model[33] was used to mimic the solvated environment. The rotation of the angles ϕ and φ, and the angles of side chains were set free during the calculations. All other parameters of the MC/SA algorithm were kept as default. Following the docking procedure, the structure of all compounds were subjected to cluster analysis with a tolerance of 1 Å for an all-atom root-mean-square (RMS) deviation from a lower-energy structure representing each cluster family. The resulting docked conformations were clustered and visualized. Interestingly, the most populated cluster was not only the one characterized by the lowest (i.e., more favorable) *AUTODOCK* energy but also the only one in which the 3D pharmacophore required interactions were satisfied by compound **1c**, as shown in Figure S8(B) (see also main text for further details).

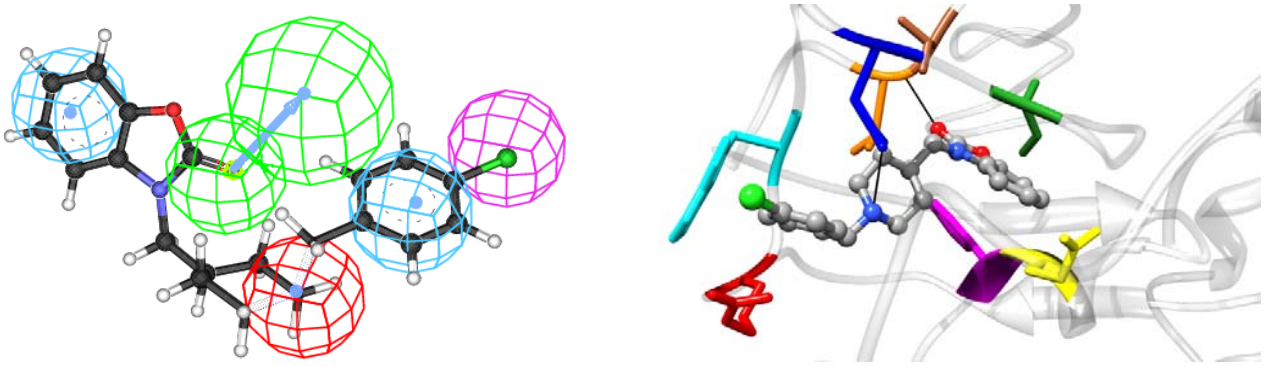

(A) (B)

Figure S8. (A) σ_1 receptor 3D pharmacophore mapping of compound **1c**. The hypothesis features are portrayed as mashed spheres, color-coded as follows: red, positive ionizable; light blue, hydrophobic aromatic; purple, hydrophobic aliphatic, light green, hydrogen bond acceptor. The last feature is actually represented as a pair of spheres (the smaller sphere represents the location of the hydrogen bond acceptor atom on the ligand and the larger one the location of an hydrogen bond donor on the receptor). (B) Compound **1c** docked into the putative binding pocket of the σ_1 3D homology model. Black lines denote polar interactions. The protein residues involved in these interactions are: Arg119 (red), Trp121 (cyan; π-π interaction, hydrophobic aromatic), Asp126 (blue; salt bridge NH-piperidine/OD2Asp, positive ionizable), Ile128 (forest green), Thr151 (sienna), Val152 (orange) (H-bond O-benzoxazolone/NH-backbone-Val; hydrogen bond acceptor), Glu172 (yellow), and Tyr173 (magenta; π-π interaction).

The same docking procedure was then applied to the entire list of compounds shown in Chart S1 (see also Table S1 for chemical formula and IUPAC nomenclature) with a twofold purpose: i)

checking the validity of the entire docking procedure on an extensive set of molecules (compounds **1a-7b**), and ii) probing the ability of the 3D σ_1 homology model to accommodate other known σ_1 ligands belonging to structurally diverse compound classes (**PTZ**, **FEN**, and **HALO**).

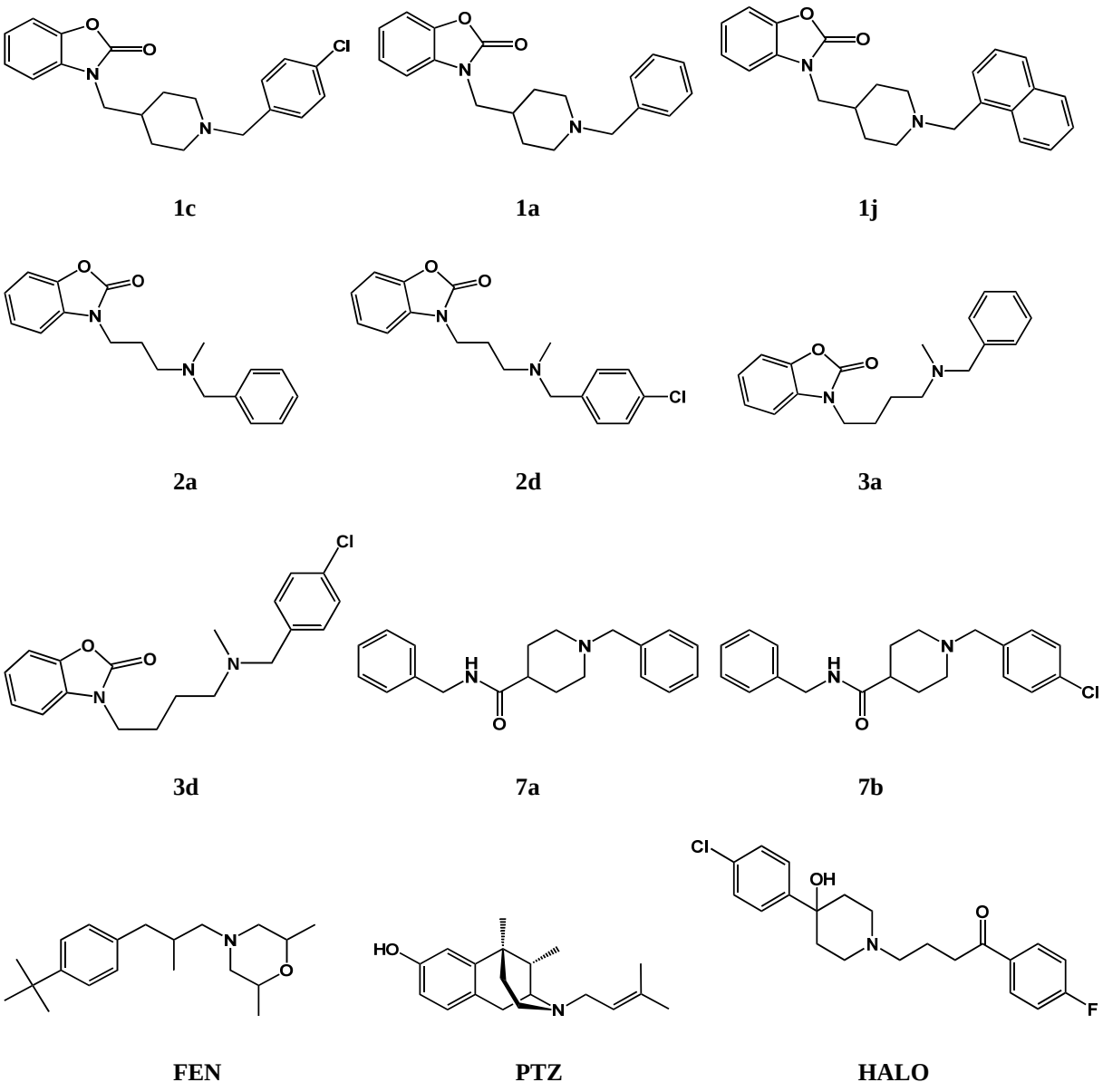

Chart S1. Chemical structures of the σ_1 ligands considered for docking, scoring, and model assisted drug design/virtual screening.

Table S1. Chemical formula and IUPAC names of the compounds

Compound	Formula	IUPAC name

1c	$C_{20}H_{21}ClN_2O_2$	3-((1-(4-Chlorobenzyl)piperidin-4-yl)methyl)benzo[d]oxazol-2(3H)-one
1a	$C_{20}H_{22}N_2O_2$	3-((1-benzylpiperidin-4-yl)methyl)benzo[d]oxazol-2(3H)-one
1j	$C_{24}H_{24}N_2O_2$	3-((1-(naphthalen-1-ylmethyl)piperidin-4-yl)methyl)benzo[d]oxazol-2(3H)-one
2a	$C_{18}H_{20}N_2O_2$	3-(3-(benzyl(methyl)amino)propyl)benzo[d]oxazol-2(3H)-one
2d	$C_{18}H_{19}ClN_2O_2$	3-(3-((4-chlorobenzyl)(methyl)amino)propyl)benzo[d]oxazol-2(3H)-one
3a	$C_{19}H_{22}N_2O_2$	3-(4-(benzyl(methyl)amino)butyl)benzo[d]oxazol-2(3H)-one
3d	$C_{19}H_{21}ClN_2O_2$	3-(4-((4-chlorobenzyl)(methyl)amino)butyl)benzo[d]oxazol-2(3H)-one
7a	$C_{20}H_{24}N_{2O}$	N,1-dibenzylpiperidine-4-carboxamide
7b	$C_{20}H_{23}ClN_{2O}$	N-benzyl-1-(4-chlorobenzyl)piperidine-4-carboxamide
FEN	$C_{20}H_{33}NO$	4-(3-(4-tert-butylphenyl)-2-methylpropyl)-2,6-dimethylmorpholine
PTZ	$C_{19}H_{27}NO$	2-dimethylallyl-5,9-dimethyl-2'-hydroxybenzomorphan
HALO	$C_{21}H_{23}ClFNO_2$	4-(4-(4-chlorophenyl)-4-hydroxypiperidin-1-yl)-1-(4-fluorophenyl)butan-1-one

S6. Ligand scoring by MM/PBSA

The resulting σ_1/**1c** complex shown in Figure S7(B), and all other best receptor/ligand complexes resulting from the automated docking procedure were further refined in *AMBER* 9 using the quenched molecular dynamics (QMD) method.[34] In this case, 1 ns molecular dynamics (MD) simulation at 300 K were employed to sample the conformational space of each ligand-receptor complex in the GB/SA continuum solvation environment.[33] The integration step was equal to 1 fs. After each ps, each system was cooled to 0 K, the structure was extensively minimized, and stored. To prevent global conformational changes of the protein, the backbone atoms of the protein binding site were constrained by an harmonic force constant of 100 kcal/Å, whereas the amino acid side chains and the ligands were allowed moving without any constraint. The best energy configuration of each complex resulting from the previous step was allowed to relax in an 80Å × 80Å × 80Å box of TIP3P water molecules.[17] The resulting systems were minimized with a gradual decrease in the position restraints of the protein atoms. Finally, to achieve electroneutrality, a suitable number of counterions neutralizing ions were added; further, the solution ionic strength was adjusted to the physiological value of 0.15 M by adding the required amounts of Na^+ and Cl^- ions. After energy minimization of the added ions for 1500 steps, keeping the protein, the ligand, and the pre-existing waters rigid, followed by an MD equilibration of the entire water/ion box with fixed solute for 5 ns, further unfavorable interactions within the structures were relieved by progressively smaller positional restraints on the solute (from 25 to 0 kcal/(mol $Å^2$)) for a total of 10 ns. Each hydrated complex system was gradually heated to 300 K in three intervals, allowing a 2 ns interval per each 100 K, and then equilibrated for 5 ns at 300 K, followed by 20 ns of data collection runs, necessary for the estimation of the free energy of binding (*vide infra*). The MD simulations were performed under the same conditions described in paragraph S4. For the calculation of the binding free energy

between σ_1 and each ligand in water, a total of 20000 snapshots were saved during the MD data collection period described above.

The binding free energy ΔG_{bind} of each σ_1 receptor/ligand complex in water was calculated according to a validated computational recipe[31,35] based on the so-called Molecular Mechanic/Poisson-Boltzmann Surface Area (MM/PBSA) ansatz, and originally proposed by Srinivasan et al.[36] Basically, an MD simulation in explicit solvent is first carried out which yields a representative ensemble of structures. The average total free energy of binding between each drug and the protein receptor can then be calculated as:

$$\Delta G_{bind} = \Delta E_{MM} + \Delta G_{solv} - T\Delta S \quad \text{(S1)}$$

where ΔG_{bind} is the binding free energy in water, ΔE_{MM} is the interaction energy between the ligand and the protein, ΔG_{sol} is the solvation free energy, and $-T\Delta S$ is the conformational entropy contribution to the binding. ΔE_{MM} is calculated from the molecular mechanics (MM) interaction energies, according to:

$$\Delta E_{MM} = \Delta E_{MM}^{ele} + \Delta E_{MM}^{vdw} \quad \text{(S2)}$$

where ΔE_{MM}^{ele} and ΔE_{MM}^{vdW} are electrostatic and van der Waals interaction energies between the ligand and the receptor, which are calculated using the *MM/PBSA* module in the *AMBER* 9 software suite. The solvation energy, ΔG_{sol}, is divided into two parts, the electrostatic contributions, ΔG_{sol}^{ele}, and all other contributions, ΔG_{sol}^{np}:

$$\Delta G_{sol} = \Delta G_{sol}^{ele} + \Delta G_{sol}^{np} \quad \text{(S3)}$$

The electrostatic contribution to the solvation free energy, ΔG_{sol}^{ele}, was estimated using the *DelPhi* software package,[37] which solves the Poisson-Boltzmann equations numerically and calculates the electrostatic energy according to the electrostatic potential. Interior and exterior dielectric constant values ε were set equal to 1 and 80, respectively. A grid spacing of 2/Å, extending 20% beyond the dimensions of the solute, was employed. The non-polar component ΔG_{sol}^{np} was obtained using the following relationship:[38] $\Delta G_{sol}^{np} = \gamma \times SA + \beta$, in which γ = 0.00542 kcal/(mol Å^2), β = 0.92 kcal/mol, and the surface area SA was estimated by means of the MSMS software.[39] The last parameter in equation (S1), i.e. the change in solute entropy upon association $-T\Delta S$, was calculated through normal-mode analysis,[40] using the *Nmode* module of *AMBER 9*. In the first step of this

calculation, an 8-Å sphere around the ligand was cut out from an MD snapshot for each ligand-protein complex. This value was shown to be large enough to yield converged mean changes in solute entropy. On the basis of the size-reduced snapshots of the complex, we generated structures of the uncomplexed reactants by removing the atoms of the protein and ligand, respectively. Each of those structures was minimized, using a distance-dependent dielectric constant $\varepsilon = 4r$, to account for solvent screening, and its entropy was calculated using classical statistical formulas and normal mode-analysis. To minimize the effects due to different conformations adopted by individual snapshots we averaged the estimation of entropy over 40 snapshots.

The entire MD simulation and data analysis procedure was optimized by integrating *AMBER 9* in *modeFRONTIER*, a multidisciplinary and multi-objective optimization and design environment.[41]

As discussed in the main text, by applying the MM/PBSA procedure described above we were able to correctly rank not only the series of compounds **1c-7b**, but also the three structurally diverse σ_1 ligands (**FEN**, **PTZ**, and **HALO**); for all these molecules, an excellent agreement ($R^2 = 0.93$) between computed and experimental affinities of these ligand series was indeed obtained, as can be inferred from the scatter plot shown in Figure S9 (see also Table 1 in main text for more details and discussion).

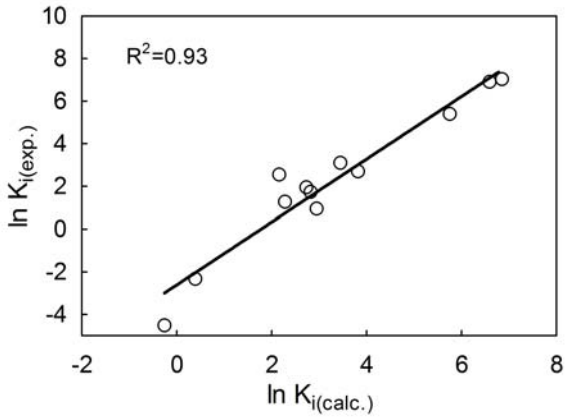

Figure S9. Linear correlation obtained between the calculated σ_1 receptor-ligand K_i values and the corresponding experimental K_i values (correlation coefficient $R^2 = 0.93$) for 12 complexes.

S7. Model-assisted drug design/virtual screening

The new 3D homology model of the σ_1 receptor was then exploited for the design of three new σ_1 ligands **EL-1**, **EL-2**, and **EL-3** (Chart S2), starting from the structure of the lead compound **1c**. In details, the chemical structures of these molecules were designed according to the following rationale: compound **EL-1** was conceived as the non-cyclic analogous of **1c**; indeed, the

benzaoxazolone moiety was replaced by a N-benzylacetamide group featuring an oxygen atom capable to fit the hydrogen bond acceptor feature (see Figure 3 of main text). The N-4-chlorobenzylpiperidine portion, essential for protein binding, was retained. Therefore, this compound was predicted to be a high affinity σ_1 ligand. On the other hand, compound **EL-2** was designed for a moderate affinity toward the receptor. In fact, despite the structure possesses all the necessary chemical requisites to satisfy the features of our models, its piperidin-1-yl-phenylmethanone scaffold yields an element of structural rigidity which, in turn, lowers the ability of the derivative to adopt the best conformational fitting in the binding site. In order to obtain a low affinity ligand, we further synthetized compound **EL-3**. The low conformational freedom of this molecule (as for **EL-2**), which hampers a complete fitting of the chemical features onto the pharmacophoric maps, and the replacement of the 4-chlorophenyl group with a piperidine ring, resulting in its inappropriate placement in a highly hydrophobic region of the receptor, concur to the quite modest affinity of this compound towards the protein. The steps **S4-S5** outline above were then repeated to predict the affinity of this small new molecular set towards the protein.

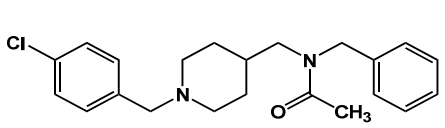

EL-1

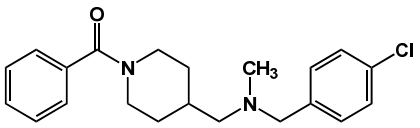

EL-2

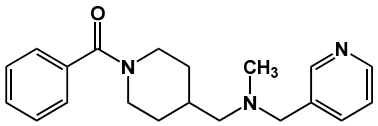

EL-3

Chart S2. Chemical structures of the new σ_1 ligands design to test the validity of the docking, scoring, and model assisted drug design/virtual screening.

Figure S10 illustrates the 3D pharmacophore mapping and the docking modes of compounds **EL-2** and **EL-3**, as resulting from the application of the entire computational procedure applied in this work.

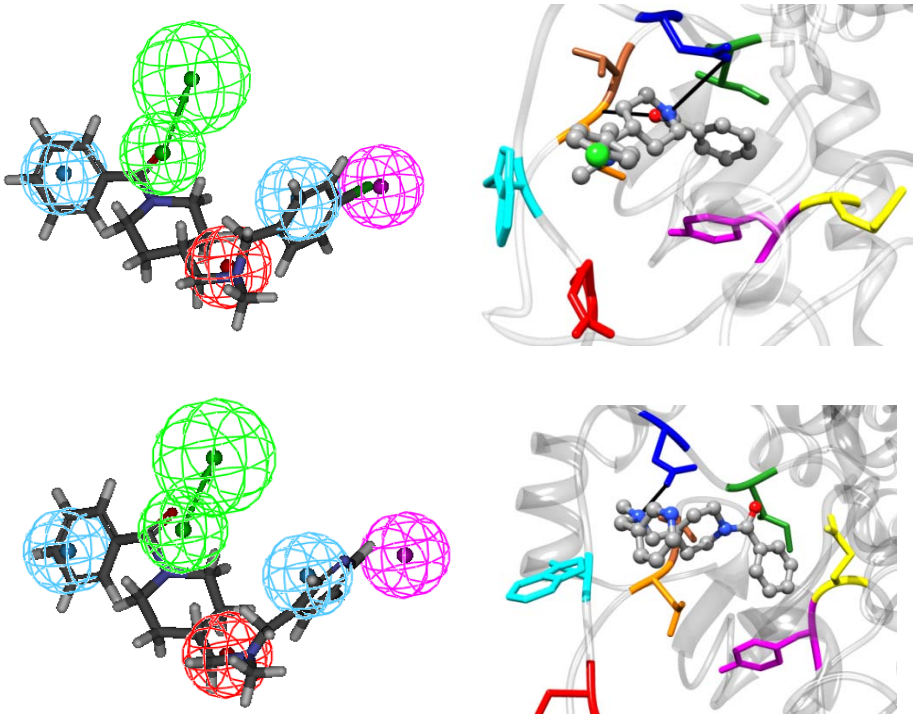

Figure S10. Right: mapping of **EL-2** (top) and **EL-3** (bottom) onto our 3D pharmacophore model developed for σ_1 ligands.[27] Left: modeled complex of the σ_1 receptor with **EL-2** (top) and **EL-3** (bottom), showing the key interactions proposed in the topographical interaction model. The main protein residues involved in these interactions are Arg119 (red), Trp121 (cyan), Asp126 (blue), Ile128 (forest green), Thr151 (sienna), Val152 (orange), Glu172 (yellow), and Tyr173 (magenta).

As reported in the main text, the three compounds indeed were ranked to have high, intermediate , and low affinity for the σ_1 receptor by the *in silico* procedure, a trend fully confirmed by the values of the corresponding experimentally determined K_i.

S8. Synthesis and characterization of compounds EL-1, EL-2, and EL-3

Compound **EL-1** was synthesized as illustrated in Scheme S1, whereas the synthetic pathway of compounds **EL-2** and **EL-3** is shown in Scheme S2.

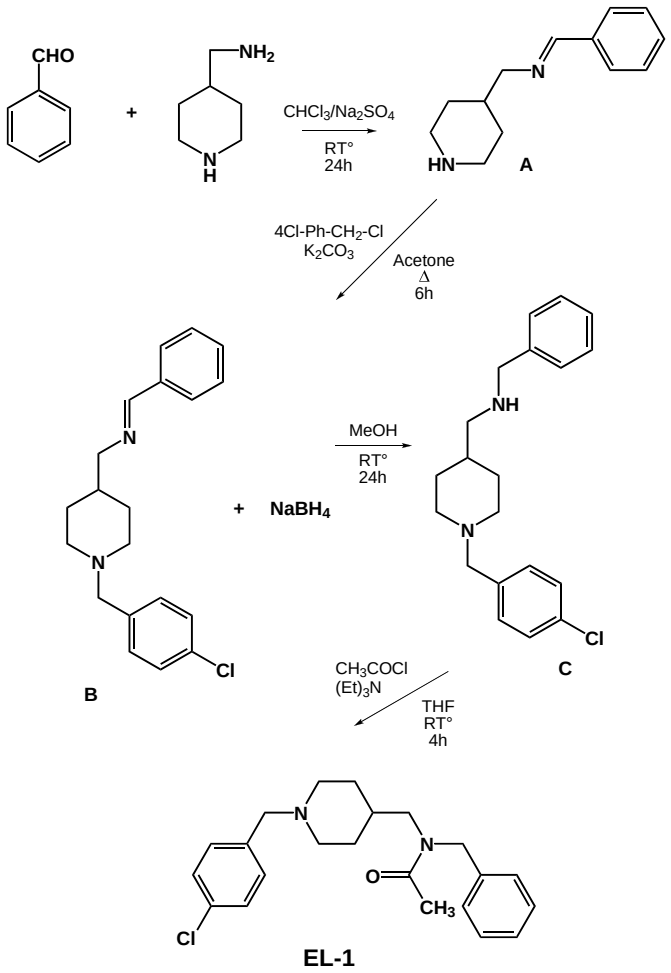

Scheme S1. Synthesis of compound **EL-1**.

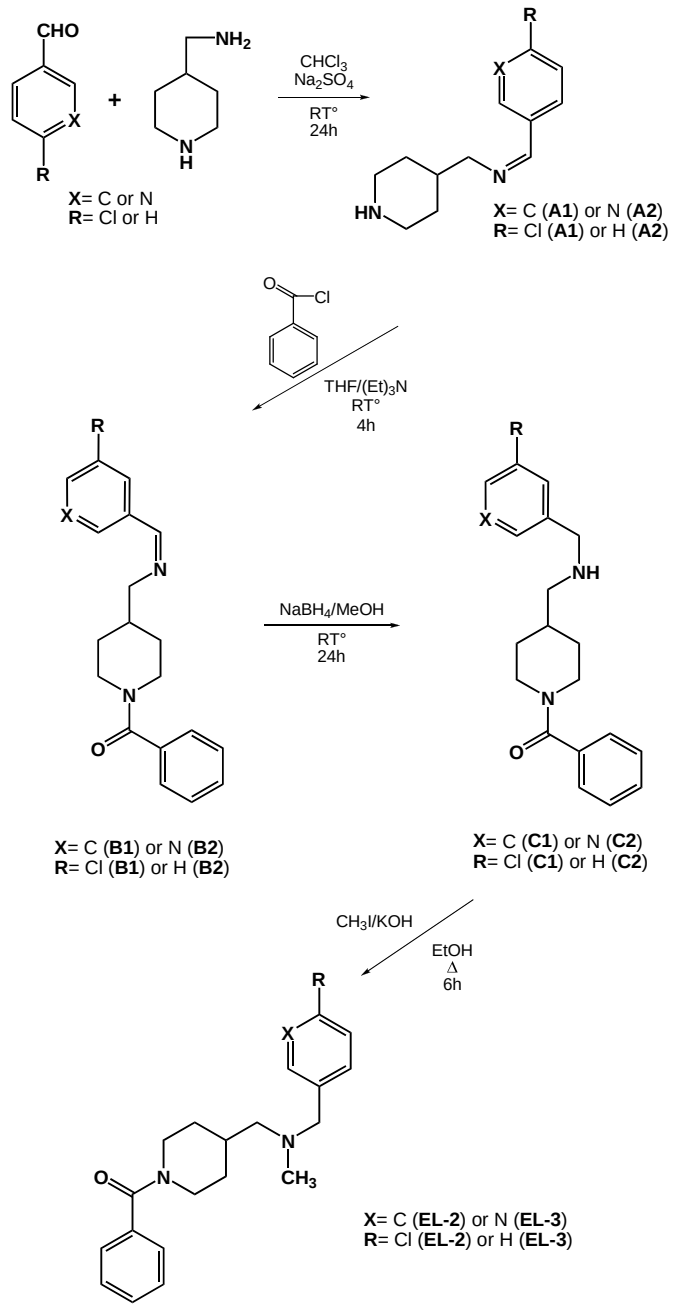

Scheme S2. Synthesis of compounds **EL-2** and **EL-3**.

Unless otherwise noted, starting materials and reagents were obtained from commercial suppliers and were used without purification. Melting points were determined with a Buchi 510 capillary apparatus and are uncorrected. Infrared spectra in Nujol mulls were recorded on a JaskoFT200 spectrophotometer. Proton nuclear magnetic resonance (1H NMR) spectra were determined on a Varian Gemini 200 spectrometer, and the chemical shifts are reported as δ (ppm) in $CDCl_3$ solution. Coupling constants J are expressed in hertz (Hz). Reaction courses and product mixtures were routinely monitored by thin-layer chromatography (TLC) on silica gel precoated F254 Merck plates. ESI-MS spectra were obtained on a PE-API I spectrometer by infusion of a solution of the

sample in MeOH. Elemental analyses (C, H, N) were performed on a Carlo Erba 1106 analyzer and were within ± 0.3 of the theoretical value.

N-Benzyliden-1-(piperidin-4-yl)methanamine **A**

To a mixture of *4-(aminomethyl)piperidine* (0.25 g, 2.19 mmol) and *benzaldehyde* (0.23 g, 2.19 mmol) in 100 ml of $CHCl_3$ was added, while stirring, Na_2SO_4 (0.33 g, 2.32 mmol) at room temperature. After 24 h, the solution was filtered to remove the inorganic salt. The organic phase was concentrated in vacuum to give compound **A** as a solid; mp 140-142°C, yield 0.42 g (96%).

I.R. cm^{-1} (nujol): 1692, 3389 cm^{-1}. ^{1}H-NMR ($CDCl_3$-TMS) ppm (δ): 1.61-1.84 (m, 6H, $H_{3,3'}$-$H_{5,5'}$-H_4, pip. + **NH** disappearing on deuteration); 2.62 (m, 2H, H_2-H_6, pip.); 3.09 (m, 2H, $H_{2'}$-$H_{6'}$, pip.); 3.48 (d, 2H, CH_2); 7.36-7.69 (m, 5H, arom.); 8.20 (s, 1H, N=**CH**-Ar). MS: m/z 203 [MH^+]. Anal. calcd. for $C_{13}H_{18}N_2$ (MW 202.30): C, 77.18; H, 8.97; N, 13.85%; found: C, 77.32; H, 9.05; N, 13.63%.

N-Benzyliden-1-(1-(4-chlorobenzyl)piperidin-4-yl)methanamine **B**

To a mixture of **A** (0.40 g, 2.01 mmol) and K_2CO_3 (0.33 g, 2.41 mmol) in 20 ml of acetone, a solution of *4-chlorobenzyl chloride* (0.32 g, 2.01 mmol) in 5 ml of acetone was added. After 4 h, the solution was filtered and the solvent was removed at reduced pressure. The crude residue was extracted with $CHCl_3$ (50 ml) and washed with distilled water (3 x 15 ml). The organic phase was dried with Na_2SO_4 and concentrated in vacuum, giving **B** as a pure yellow oil; yield 0.48 g (82%).

I.R. cm^{-1} (nujol): 1640. ^{1}H-NMR ($CDCl_3$-TMS) ppm (δ): 1.58-1.99 (m, 5H, $H_{3,3'}$-$H_{5,5'}$-H_4, pip.); 2.16-2.28 (m, 2H, H_2-H_6, pip.); 2.81-3.02 (m, 2H, $H_{2'}$-$H_{6'}$, pip.) 3.46 (d, 2H, CH_2); 3.63 (s, 2H, N-**CH_2**-phenyl); 7.25-7.79 (m, 9H, arom.); 8.27 (s, 1H, N=**CH**-Ar). MS: m/z 327 [MH^+] 328 [MH^++2]. Anal. calcd. for $C_{20}H_{23}ClN_2$ (MW 326.86): C, 73.49; H, 7.09; N, 8.57%; found: C, 73.22; H, 7.18; N, 8.69%.

N-Benzil-1-(1-(4-clorobenzil)piperidin-4-il)metanammina **C**

To a mixture of **B** (0.50 g, 1.71 mmol) in 25 ml of MeOH, was slowly added *$NaBH_4$* (0.11 g, 3.42 mmol). After stirring overnight, the solution was concentrated in vacuum and extracted with AcOEt (30 ml). The organic phase was washed with distilled water (3 x 15 ml) and then evaporated under reduced pressure, yielding **C** as a pure pale oil; yield 0.44 g (78%).

I.R. cm^{-1} (nujol): 3261. ^{1}H-NMR ($CDCl_3$-TMS) ppm (δ): 1.38-1.71 (m, 5H, $H_{3,3'}$-$H_{5,5'}$-H_4, pip.); 1.89-2.11 (m, 3H, H_2-H_6, pip. + **NH** disappearing on deuteration); 2.51 (d, 2H, CH_2); 2.78-2.94 (m,

2H, $H_{2'}$-$H_{6'}$, pip.); 3.50 (s, 2H, N-**CH_2**-phenyl); 3.79 (s, 2H, NH-**CH_2**-phenyl); 7.23-7.62 (m, 9H, arom.). MS: m/z 329 [MH^+] 331 [MH^++2]. Anal. calcd. for $C_{20}H_{25}ClN_2$ (MW 328.88): C, 73.04; H, 7.66; N, 8.52%; found: C, 72.89; H, 7.90; N, 8.82%.

N-Benzyl-N-((1-(4-chlorobenzyl)piperidin-4-yl)methyl)acetamide **EL-1**

To a solution of **C** (0.62 g, 1.90 mmol) and *triethylamine* (0.23 g, 2.28 mmoli) in 10 ml of THF, a solution of acetyl chloride (0.15 g, 1.90 mmol) in 5 ml of THF was added cooling and drop wise. After 5 h, the solvent was removed at reduced pressure and the residue was extracted with $CHCl_3$. The organic phase was washed, dried and concentrated in vacuum, giving **EL-1** as a chromatographic and colorless oil; yield 0.49 g (69%).

I.R. cm^{-1} (nujol): 1741 cm^{-1}. ^{1}H-NMR ($CDCl_3$-TMS) ppm (δ): 1.30-1.77 (m, 5H, $H_{3,3'}$-$H_{5,5'}$-H_4, pip.); 1.84-2.08 (m, 2H, H_2-H_6, pip.); 2.30 (s, 3H, -CO-**CH_3**); 2.75-3.00 (m, 2H, $H_{2'}$-$H_{6'}$, pip.); 3.26 (d, 2H, CH_2); 3.54 (s, 2H, N-**CH_2**-phenyl); 4.53 (s, 2H, CO-N-**CH_2**-phenyl); 7.12-7.52 (m, 9H, arom.). MS: m/z 371 [MH^+] 373 [MH^++2]. Anal. calcd. for $C_{22}H_{27}ClN_2O$ (MW 370.92): C, 71.24; H, 7.34; N, 7.55%; found: C, 71.39; H, 7.15; N, 7.68%.

N-(4-Chlorobenzyliden)-1-(piperidin-4-yl)methanamine **A1**

To a stirring solution of *4-(aminomethyl)piperidine* (0.25 g, 2.19 mmol) and *4-chlorobenzaldehyde* (0.31 g, 2.19 mmol) in 100 ml of $CHCl_3$, Na_2SO_4 (0.33 g, 2.32 mmol) was added at room temperature. After 24 h, the solution was filtered to remove the inorganic salt. The organic phase was concentrated in vacuum to give compound **A1** as a light-brown solid; mp 135-137°C, yield 0.42 g (81%).

I.R. cm^{-1} (nujol): 1690, 3393 cm^{-1}. ^{1}H-NMR ($CDCl_3$-TMS) ppm (δ): 1.60-1.89 (m, 6H, $H_{3,3'}$-$H_{5,5'}$-H_4, pip. + **NH** disappearing on deuteration); 2.65 (m, 2H, H_2-H_6, pip.); 3.15 (m, 2H, $H_{2'}$-$H_{6'}$, pip.); 3.46 (d, 2H, CH_2); 7.30-7.70 (m, 4H, arom.); 8.22 (s, 1H, N=**CH**-Ar). MS: m/z 237 [MH^+] 239 [MH^++2]. Anal. Calcd. for $C_{13}H_{17}ClN_2$ (MW 236.74): C, 65.95; H, 7.24; N, 11.83%; found: C, 66.11; H, 7.16; N, 11.72%.

Compound **A2** was synthesized according to the same procedure using *nicotinaldehyde*.

N-(pyridin-3-ylmethylen)-1-(piperidin-4-yl)methanamine **A2**

I.R. cm^{-1} (nujol): 1680, 3387 cm^{-1}. ^{1}H-NMR ($CDCl_3$-TMS) ppm (δ): 1.39-1.95 (m, 5H, $H_{3,3'}$-$H_{5,5'}$-H_4, pip.); 2.30 (s broad, 1H, **NH** disappearing on deuteration); 2.71 (m, 2H, H_2-H_6, pip.); 3.10 (m, 2H, $H_{2'}$-$H_{6'}$, pip.); 3.52 (d, 2H, CH_2); 7.36-7.92 (m, 3H, arom.); 8.30 (s, 1H, N=**CH**-Ar); 8.86 (m,

1H, arom.). MS: m/z 204 [MH^+]. Anal. calcd. for $C_{12}H_{17}N_3$ (MW 203.28): C, 70.90; H, 8.43; N, 20.67%; found: C, 70.79; H, 8.48; N, 20.73%.

(4-((4-Chlorobenzylidenamino)methyl)piperidin-1-yl)(phenyl)methanone **B1**

To a mixture of **A1** (0.44 g, 1.87 mmol) and *triethylamine* (0.23 g, 2.28 mmol) in 10 ml of THF, a solution of *benzoyl chloride* (0.26 g, 1.87 mmol) in 5 ml of THF was added drop wise at 0°C. After 4h, the solution was concentrated under reduced pressure and $CHCl_3$ (30 ml) was added. The organic phase was washed with distilled water (3 x 15 ml), dried with Na_2SO_4 and concentrated in vacuum to obtain **B1** as a pure oil; yield 0.51 g (80%).

I.R. cm^{-1} (nujol): 1645, 1718 cm^{-1}. ^{1}H-NMR ($CDCl_3$-TMS) ppm (δ): 1.58-1.92 (m, 5H, $H_{3,3'}$-$H_{5,5'}$-H_4, pip.); 2.98-3.21 (m, 4H, $H_{2,2'}$-$H_{6,6'}$, pip.) ; 3.58 (d, 2H, CH_2); 7.38-8.06 (m, 9H, arom.); 8.25 (s, 1H, N=**CH**-Ar). MS: m/z 341 [MH^+] 343 [MH^++2]. Anal. calcd. for $C_{20}H_{21}ClN_2O$ (MW 340.85): C, 70.48; H, 6.21; N, 8.22%; found: C, 70.61; H, 6.07; N, 8.44%.

Compound **B2** was obtained following the same approach, starting from **A2**.

Phenyl(4-((pyridin-3-ylmethylenamino)methyl)piperidin-1-yl)methanone **B2**

I.R. cm^{-1} (nujol): 1650, 1718 cm^{-1}. ^{1}H-NMR ($CDCl_3$-TMS) ppm (δ): 1.51-1.99 (m, 5H, $H_{3,3'}$-$H_{5,5'}$-H_4, pip.); 2.81-3.08 (m, 4H, $H_{2,2'}$-$H_{6,6'}$, pip.) ; 3.52 (d, 2H, CH_2);); 7.28-8.04 (m, 8H, arom.); 8.11 (s, 1H, N=**CH**-Ar); 8.60 (m, 1H, arom.). MS: m/z 308 [MH^+]. Anal. calcd. for $C_{19}H_{21}N_3O$ (MW 307.39): C, 74.24; H, 6.89; N, 13.67%; found: C, 74.16; H, 6.80; N, 13.85%.

(4-((4-Chlorobenzylamino)methyl)piperidin-1-yl)(phenyl)methanone **C1**

To a mixture of **B1** (0.58 g, 1.69 mmol) in 25 ml of MeOH, *$NaBH_4$* (0.13 g, 3.47 mmol) was slowly added. After stirring overnight, the solution was concentrated in vacuum and extracted with AcOEt (30 ml). The organic phase was washed with distilled water (3 x 15 ml) and then evaporated under reduced pressure, yielding **C1** as a pure and colorless oil; yield 0.41 g (71%).

I.R. cm^{-1} (nujol): 1723, 3258 cm^{-1}. ^{1}H-NMR ($CDCl_3$-TMS) ppm (δ): 1.28-1.72 (m, 5H, $H_{3,3'}$-$H_{5,5'}$-H_4, pip.); 2.01 (s broad, 1H, **NH** disappearing on deuteration); 2.52 (d, 2H, CH_2); 2.80-2.99 (m, 4H, $H_{2,2'}$-$H_{6,6'}$, pip.); 3.77 (s, 2H, N-**CH_2**-aryl) 7.25-7.41 (m, 9H, arom.). MS: m/z 343 [MH^+] 345 [MH^++2]. Anal. calcd. for $C_{20}H_{23}ClN_2O$ (MW 342.86): C, 70.06; H, 6.76; N, 8.17%; found: C, 69.83; H, 6.91; N, 8.30%.

Compound **C2** was synthesized according to the same procedure starting from **B2**.

(4-((Pyridin-3-ylmethylamino)methyl)piperidin-1-yl)(phenyl)methanone **C2**

I.R. cm^{-1} (nujol): 1719, 3265 cm^{-1}. ^{1}H-NMR ($CDCl_3$-TMS) ppm (δ): 1.26-1.60 (m, 5H, $H_{3,3'}$-$H_{5,5'}$-H_4, pip.); 1.85 (s broad, 1H, **NH** disappearing on deuteration); 2.58 (d, 2H, CH_2); 2.69-3.04 (m, 4H, $H_{2,2'}$-$H_{6,6'}$, pip.); 3.81 (s, 2H, N-**CH_2**-aryl) 7.27-7.78 (m, 8H, arom.); 8.52 (m, 1H, arom.). MS: m/z 310 [MH^+]. Anal. calcd. for $C_{19}H_{23}N_3O$ (MW 309.41): C, 73.76; H, 7.49; N, 13.58%; found: C, 73.85; H, 7.69; N, 13.32%.

(4-(((4-Chlorobenzyl)(methyl)amino)methyl)piperidin-1-yl)(phenyl)methanone **EL-2**

Compound **C1** (0.20 g, 0.58 mmol) was dissolved in 10 ml of EtOH, KOH (0.07 g, 1.22 mmol) and *CH_3I* (0.08 g, 0.58 mmol) were then added. The reaction was heated at reflux temperature and carried out under stirring. After 6h, EtOH was evaporated under reduced pressure and the crude residue was extracted with $CHCl_3$ (20 ml). the organic phase was washed with distilled water (3 x 10 ml), dried with Na_2SO_4 and concentrated in vacuum, giving **EL-2** as a pure pale oil; yield 0.16 g (77%).

I.R. cm^{-1} (nujol): 1722 cm^{-1}. ^{1}H-NMR ($CDCl_3$-TMS) ppm (δ): 1.26-1.80 (m, 5H, $H_{3,3'}$-$H_{5,5'}$-H_4, pip.); 2.17 (d, 2H, CH_2); 2.22 (s, 3H, CH_3); 2.71-3.02 (m, 4H, $H_{2,2'}$-$H_{6,6'}$, pip.); 3.75 (s, 2H, N-**CH_2**-aryl) 7.26-7.49 (m, 9H, arom.). MS: m/z 357 [MH^+] 359 [MH^++2]. Anal. calcd. for $C_{21}H_{25}ClN_2O$ (MW 356.89): C, 70.67; H, 7.06; N, 7.85%; found: C, 70.53; H, 7.16; N, 7.78%.

Compound **EL-3** was synthesized in analogous way using **C2**.

(4-((Methyl(pyridin-3-ylmethyl)amino)methyl)piperidin-1-yl)(phenyl)methanone **EL-3**

I.R. cm^{-1} (nujol): 1723 cm^{-1}. ^{1}H-NMR ($CDCl_3$-TMS) ppm (δ): 1.28-1.81 (m, 5H, $H_{3,3'}$-$H_{5,5'}$-H_4, pip.); 2.19 (d, 2H, CH_2); 2.23 (s, 3H, CH_3); 2.72-3.05 (m, 4H, $H_{2,2'}$-$H_{6,6'}$, pip.); 3.49 (s, 2H, N-**CH_2**-aryl) 7.27-7.75 (m, 8H, arom.); 8.58 (m, 1H, arom.). MS: m/z 324 [MH^+]. Anal. calcd. for $C_{20}H_{25}N_3O$ (MW 323.43): C, 74.27; H, 7.79; N, 12.99%; found: C, 74.16; H, 7.93; N, 12.87%.

S9. Pharmacology

Radioligand Binding Assays. Radioligand binding assays, based upon a modified version of the method[42] originally proposed by Hellewell,[43] were performed using rat liver membranes. Accordingly, 250 μg of rat liver homogenate was incubated for 120 min at 37 °C with 1 nM [3H]-(+)-pentazocine (PerkinElmer, specific activity 34.9 Ci/mmol) in 50mM Tris-HCl, pH 8.0, 0.5 mL final volume. 10 μM haloperidol was employed to define eventual nonspecific binding. The

reaction was stopped by vacuum filtration through GF/B glass-fiber filters presoacked with 0.5% polyethylenimine, followed by rapid washing with 2 mL of ice-cold buffer. The filters were placed in 3 mL of scintillation cocktail, and the radioactivity was determined by liquid scintillation counting. For competition studies, at least 11 different concentrations of each ligand under investigation were employed. Three increasing concentrations of unlabeled (+)-pentazocine were always included as internal control. All compounds were prepared as fresh 10 mM stock solutions in 100% DMSO and diluted with Tris-HCl buffer the same day of the assay. The final DMSO concentration in the incubation tubes was maintained at 0.1%. Competition data for two to four separate determinations performed in duplicate were averaged by fitting to a four-parameter curve by means of the SigmaPlot software. Calculated IC_{50} values are reported as mean values ± SEM. The corresponding K_i values were obtained by the Cheng-Prusoff equation, as previously reported.[44]

References

1. K. Hofmann, W. Stoffel, *Biol. Chem. Hoppe Seyler* **1993**, *347*, 166-170.
2. J. J. Ward, J. S. Sodhi, L. J. McGuffin, B. F. Buxton, D. T. Jones, *J. Mol. Biol*. **2004**, *337*, 635-645.
3. B. Rost B, G. Yachdav, J. Liu. *Nucleic Acids Res*. **2004**, *32*, 321-326.
4. G. E. Tusnady, I. Simon, *Bioinformatics* **2001**, *17*, 849-850.
5. a) R. Ambrish, K. Alper, Z. Yang, *Nature Protocols* **2010**, *5*, 725-738; b) Z. Yang, *BMC Bioinformatics*, **2008**, *9*, 40.
6. E. Gasteiger, A. Gattiker, C. Hoogland, I. Ivanyi, R. D. Appel, A. Bairoch, *Nucleic Acids Res*. **2003**, *31*, 3784-3788.
7. C. Bauvois, L. Jacquamet, A. L. Huston, F. Borel, G. Feller, J. L. Ferrer, *J. Biol. Chem*. **2008**, *283*, 23315-23325.
8. M. J. Theisen, S. L. Sanda, S. L. Ginell, C. Benning, R. M. Garavito, to be published.
9. S. Tanaka, H. Matsumura, Y. Koga, K. Takano, S. Kanaya, *J. Mol. Biol*. **2007**, *372*, 1055-1069.
10. M. Kato, J. Li, J. L. Chuang, D. T. Chuang, *Structure* **2007**, *15*, 992-1004.
11. E. F. Pettersen, T. D. Goddard, C. C. Huang, G. S. Couch, D. M. Greenblatt, E. C. Meng, T. E. Ferrin, *J. Comput. Chem*. **2004**, *25*, 1605-1612.
12. R. A. Laskowski, M. W. MacArthur, D. S. Moss, J. M. Thornton, *J. Appl. Cryst*. **1993**, *26*, 283-291.
13. G. Vriend, *J. Mol. Graph*. **1990**, *8*, 52-56.
14. M. J. Sippl, J. *Comput.-Aided Mol. Des*. **1993**, *7*, 473-501.
15. B. Jojart, T. A. Martinek, *J. Comput. Chem*. **2007**, *28*, 2051-2058.
16. D. A. Case, T. A. Darden, T. E. Cheatham III *et al*., *AMBER 9*, **2006**, University of California, San Francisco, CA, USA.
17. W. L. Jorgensen, J. Chandrasekhar, J. D. Madura, R. W. Impey, M. L. J. Klein, *J. Chem. Phys*. **1983**, *79*, 926-935.
18. Y. Duan, C. Wu, S. Chowdhury, M. C. Lee, G. Xiong, W. Zhang, R. Yang, P. Cieplak, R. Luo, T. Lee, *J. Comput. Chem*. **2003**, *24*, 1999-2012.
19. H. J. C. Berendsen, J. P. M. Postma, W. F. Van Gunsteren, A. DiNola, J. R. Haak, *J. Chem. Phys*. **1984**, *81*, 3684-3690.

20. J. P. Ryckaert, G. Ciccotti, H. J. C. Berendsen, *J. Comput. Phys*. **1977**, *23*, 327-341.
21. A. Toukmaji, C. Sagui, J. Board, T. Darden, *J. Chem. Phys*. **2000**, *113*, 10913-10927.
22. V. B. Chen, W. B. Arendall III, J. J. Headd, D. A. Keedy, R. M. Immormino, G. J. Kapral, L. W. Murray, J. S. Richardson, D. C. Richardson, *Acta Crystallographica* **2010**, *D66*, 12-21.
23. R. Luthy, J. U. Bowie, D. Eisenberg, *Nature* **1992**, *356*, 83-85.
24. D. Baker, A. Sali, *Science* **2001**, *294*, 93-96.
25. B. Rost, *Protein Engng*. **1999**, *12*, 85-94.
26. P. Seth, M. E. Ganapathy, S. J. Conway, C. D. Bridges, S. B. Smith, P. Casellas, V. Ganapathy, *Biochim. Biophys. Acta* **2001**, *1540*, 59-67.
27. a) D. Zampieri, M. G. Mamolo, E. Laurini, C. Florio, C. Zanette, M. Fermeglia, P. Posocco, M. S. Paneni, S. Pricl, L. Vio, *J. Med. Chem*. **2009**, *52*, 5380-5393; b) , E. Laurini, D. Zampieri, M. G. Mamolo, L. Vio, C. Zanette, C. Florio, P. Posocco, M. Fermeglia, S. Pricl, *Bioorg. Med. Chem. Lett*. **2010**, *20*, 2954-2957.
28. A. Pal, A. R. Hajipour, D. Fontanilla, S. Ramachandran, U. B. Chu, T. Mavlyutov, A. E. Ruoho, *Mol. Pharmacol*. **2007**, *72*, 921-933.
29. E. J. Cobos, J. M. Entrena, F. R. Nieto, C. M. Cendan, E. D. Pozo, *Curr. Neuropharmacol*. **2008**, *6*, 344-366.
30. a) G. M. Morris, R. Huey, W. Lindstrom, M. F. Sanner, R. K. Belew, D. S. Goodsell, A. J. Olson, *J. Comput. Chem*. **2009**, *30*, 2785-2791; b) R. Huey, G. M. Morris, A. J. Olson, *J. Comput. Chem*. **2009**, *28*, 1145-1152; c) Osterberg, F., G. M. Morris, M. F. Sanner, A. J. Olson, D. S. Goodsell, *Proteins* **2002**, *46*, 34-40.
31. See, for instance: a) G. Giliberti, C. Ibba, E. Marongiu, R. Loddo, M. Tonelli, V. Boido, E. Laurini, P. Posocco, M. Fermeglia, S. Pricl, *Bioorg. Med. Chem.* **2010**, *18*, 6055-6068; b) M. Tonelli, V. Boido, P. La Colla, R. Loddo, P. Posocco, M. S. Paneni, M. Fermeglia, S. Pricl, *Bioorg. Med. Chem.* **2010**, *18*, 23042316; c) A. Carta, S. Pricl, S. Piras, M. Fermeglia, P. La Colla, R. Loddo, *Eur. J. Med. Chem.* **2009**, *44*, 5117-5122; d) M. Tonelli, I. Vazzana, B. Tasso, V. Boido, F. Sparatore, M. Fermeglia, M. S. Paneni, P. Posocco, S. Pricl, P. La Colla, C. Ibba, B. Secci, G. Collu, R: Loddo, *Bioorg. Med. Chem*. **2009**, *17*, 4425-4440 and references therein.
32. E. L. Mehler, T. Solmajer, *Protein Eng*. **1991**, *4*, 903-910.
33. a) A. Onufriev, D. Bashford, D. A. Case, *J. Phys. Chem. B* **2000**, *104*, 3712-3720; b) M. Feig, A. Onufriev, M. Lee, W. Im, D. A. Case, C. L. Brooks III. *J. Comput. Chem*. **2004**, 25, 265-284.
34. a) F. Felluga, G. Pitacco, E. Valentin, A. Coslanich, M. Fermeglia, M. Ferrone, S. Pricl, *Tetrahedron: Asymmetry* **2003**, *14*, 3385-3399; b) V. Frecer, M. Kabelac, P. De Nardi, S. Pricl, S. Miertus, *J. Mol. Graph. Model*. **2004**, *22*, 209-220.
35. For a recent selection of MM/PBSA calculations from our group see: a) M.A. Pierotti, E. Tamborini, T. Negri, S. Pricl, S. Pilotti, *Nat. Rev. Clin. Oncol*. **2011**, *8*, 161-170; b) P. Dileo, S. Pricl, E. Tamborini, T. Negri, S. Stacchiotti, A. Gronchi, P. Posocco, E. Laurini, P. Coco, E. Fumagalli, P. G. Casali, S. Pilotti, *Int. J. Cancer* **2011**, *128*, 983-990; c) G. M. Pavan, P. Posocco, A. Tagliabue, M. Maly, A. Malek, A. Danani, E. Ragg, C. V. Catapano, S. Pricl, *Chemistry* **2010**, *16*, 7781-7795; d) S. P. Jones, G. M. Pavan, A. Danani, S. Pricl, D. K. Smith, *Chemistry* **2010**, *16*, 4519-4532; e) M. A. Pierotti, T. Negri; E. Tamborini, F. Perrone, S. Pricl, S. Pilotti, *Mol. Oncol*. 2010, 4, 19-37; f) G. M. Pavan, A. Danani, S. Pricl, D. K. Smith, *J. Am. Chem. Soc*. **2009**, *131*, 9686-9694; g) D. Zampieri, M. G. Mamolo, E. Laurini, M. Fermeglia, P. Posocco, S. Pricl, E. Banfi, G. Scialino, L. Vio, *Bioorg. Med. Chem*. **2009**, *17*, 4693-4707, and references therein.
36. J. Srinivasan, T. E. Cheatham III, P. Cieplak, P. A. Kollman, D. A. Case, *J. Am. Chem. Soc*. 1998, 120, 9401-9409.
37. M. K. Gilson, K. A. Sharp, B. H. Honig, B. H. *J. Comput. Chem*. **1988**, *9*, 327-335.
38. D. Sitkoff, K.A. Sharp, B. H. Honig, *J. Phys. Chem*. **1994**, *98*, 1978-1988.
39. M. F. Sanner, A. J. Olson, J. C. Spehner, *Biopolymers* **1996**, *38*, 305-320.

40. E. B. Wilson, J.C. Decius, P.C. Cross, *Molecular Vibrations*. New York, NY:McGraw-Hill; **1995**.
41. http://www.esteco.com/home/mode_frontier/mode_frontier.html.
42 D. Zampieri, M. G. Mamolo, E. Laurini, C. Zanette, C. Florio, S. Collina, M. Urbano, O. Azzolina, L. Vio, *Eur. J. Med. Chem*. **2009**, *44*, 124-30.
43 S. B. Hellewell, A. Bruce, G. Feinstein, J. Orringer, W. Williams, W. D. Bowen, *Eur. J. Pharmacol*. **1994**, *268*, 9-18.
44 M. G: Mamolo, D. Zampieri, C. Zanette, C. Florio, S. Collina, M. Urbano, O. Azzolina, L. Vio, *Eur. J. Med. Chem*. **2008**, *43*, 2073-2081.